

Article

# Impact of Silicon Carbide Devices on the Powertrain Systems in Electric Vehicles

Xiaofeng Ding \*, Jiawei Cheng and Feida Chen

School of Automation Science and Electrical Engineering, Beihang University, Beijing 100191, China; chengjiawei0218@126.com (J.C.); dage820@buaa.edu.cn (F.C.)

\* Correspondence: dingxiaofeng@buaa.edu.cn; Tel.: +86-10-8233-9498

Academic Editor: Rui Xiong

Received: 7 February 2017; Accepted: 11 April 2017; Published: 14 April 2017

**Abstract:** The DC/DC converters and DC/AC inverters based on silicon carbide (SiC) devices as battery interfaces, motor drives, etc., in electric vehicles (EVs) benefit from their low resistances, fast switching speed, high temperature tolerance, etc. Such advantages could improve the power density and efficiency of the converter and inverter systems in EVs. Furthermore, the total powertrain system in EVs is also affected by the converter and inverter system based on SiC, especially the capacity of the battery and the overall system efficiency. Therefore, this paper investigates the impact of SiC on the powertrain systems in EVs. First, the characteristics of SiC are evaluated by a double pulse test (DPT). Then, the power losses of the DC/DC converter, DC/AC inverter, and motor are measured. The measured results are assigned into a powertrain model built in the Advanced Vehicle Simulator (ADVISOR) software in order to explore a direct correlation between the SiC and the performance of the powertrain system in EVs, which are then compared with the conventional powertrain system based on silicon (Si). The test and simulation results demonstrate that the efficiency of the overall powertrain is significantly improved and the capacity of the battery can be remarkably reduced if the Si is replaced by SiC in the powertrain system.

**Keywords:** DC/DC converters; DC/AC inverters; silicon carbide (SiC); electric vehicles (EV); powertrain system; battery

## 1. Introduction

Because of the global energy crisis and environmental pollution, the past decade has witnessed the rapid development of new energy vehicle technologies, such as Electric Vehicles (EVs), Hybrid Electric Vehicles (HEVs), Plug-in Hybrid Electric Vehicles (PHEVs), etc. As a result, more and more companies that produce transportation vehicles are developing new technologies for EVs/HEVs/PHEVs [1–11]. The main challenge of EVs/HEVs/PHEVs development remains the limited cruising range due to the small battery capacity and the long charging times according to the available battery charging technologies, especially for pure electric vehicles [3–7]. Hence, it is important to maximize the efficiency of each component in the powertrain system of EVs [8]. The high efficiency of the system will distinctly reduce the burden of the battery and extend the cruising range.

A typical powertrain system in an EV and the corresponding losses are shown in Figure 1. The main contributions of the total losses are copper and iron losses in a permanent magnet synchronous machine (PMSM), and switching and conduction losses of switching devices in both the DC/DC converter and inverter, respectively.

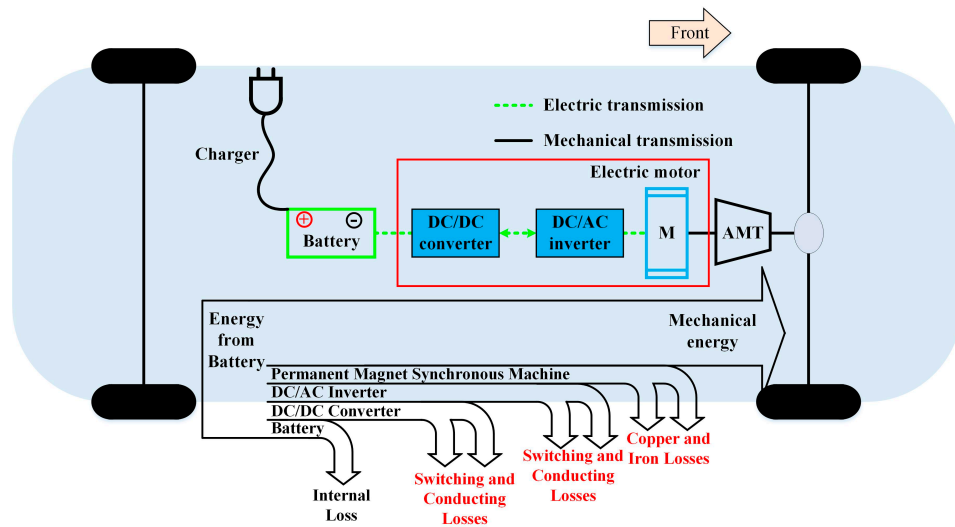


Figure 1. The components of the powertrain system in an electric vehicle (EV) and the corresponding losses.

Currently, the conventional insulated-gate bipolar transistor (IGBT) or Si metal-oxide-semiconductor field-effect transistor (MOSFET) technologies based on silicon (Si) material dominate the semiconductor fields in the application of power converters and inverters. However, the Si IGBT/MOSFET is now reaching the material’s theoretical limits. Higher efficiency, higher power density, and higher temperature application are the urgent requirements in traction converters and inverters of EVs. Recently, wide band-gap (WBG) silicon carbide (SiC) MOSFET has exhibited great potential to replace Silicon (Si) as the dominant transistor technology according to its extreme advantages, such as faster switching speed, lower voltage-drop, higher operating temperature, etc. [1,2,12–17]. Such outstanding characteristics of SiC are due to the advantages of its material and structure, such as higher electron velocity, higher energy gap, higher thermal conductivity, etc., which are shown in Figure 2. As a result, a motor drive system, which consists of a converter plus an inverter, based on SiC devices can provide higher efficiency and higher power density in comparison with their Si counterparts [9,10,18–21].

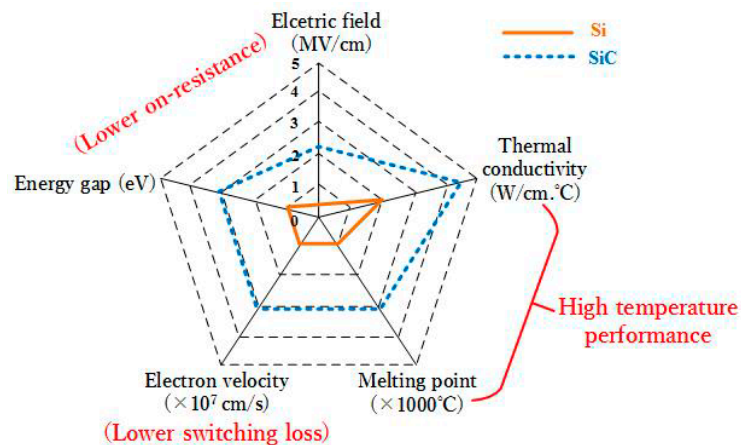


Figure 2. The components of the powertrain system in an EV and the corresponding losses.

Much research involving SiC has been widely conducted by many researchers [1,2,9–23]. Most of the work reflects an enormous effort investigating the switching and conduction losses of SiC [1,9,12,23]. For example, Ref. [22,23] developed a loss model of SiC, and both the conduction loss and switching loss of SiC are less than that of Si. The efficiency of the inverter based on SiC is 99.1% while the efficiency of the Si-inverter is 97.1%. The above work mostly focuses on the losses of the SiC-inverter

or converter. However, the impact of SiC on the overall-powertrain system has not been explored systematically yet.

Therefore, this paper comprehensively investigates the impact of SiC on the powertrain systems in EVs. First, the characteristics of SiC are measured by a double pulse test (DPT). Then, the power losses of the DC/DC converter, DC/AC inverter, and motor are tested. The experimental results are assigned into a powertrain model built in the Advanced Vehicle Simulator (ADVISOR) software in order to explore a direct correlation between the SiC and the EV's battery capacity as well as the overall powertrain system efficiency. The SiC results are compared with the conventional powertrain system based on Si.

The remainder of this paper is organized as follows. In Section 2, the characteristics of SiC and Si are evaluated. In Section 3, the efficiencies of the DC/DC converter, DC/AC inverter, and motor are measured. In Section 4, simulations of the powertrain are implemented in ADVISOR. Conclusions are drawn in the final section.

## 2. SiC Device Characterization

The characteristics of a SiC power device are investigated experimentally in this Section, and compared with the Si counterparts. Both dynamic and static characteristics are tested. The test bench adopts a double pulse test (DPT), which is the widely accepted test method. Figure 3 shows the DPT test bench. A high accuracy current probe and a high accuracy voltage probe are used, namely a current probe TCPA300 plus TCP303 and a voltage probe P5100A.

The switching transition waveforms of SiC and Si are described in Figures 4 and 5, respectively. Both the turn-on and turn-off speed of SiC are faster than the Si counterparts. The quantified results are summarized in Table 1. The turn-on time of SiC is 85 ns while the turn-on time of Si is 143 ns at 25 °C. Meanwhile, the turn-on time of SiC is 79 ns while the turn-on time of Si is 145 ns at 175 °C. The turn-on times of both SiC and Si are around a constant value as the temperature changes. However, the turn-off time of Si is 752 ns at 175 °C, which is almost twice the value of 328 ns when Si operates at 25 °C. The turn-off time of SiC is not sensitive to the change of temperature, as well as its turn-on time. Such characteristics indicate that the switching loss of SiC is not increasing as the temperature rises. However the switching loss of Si incredibly rises as the temperature increases.

The variation tendencies of the voltage-drops of SiC and Si are different with their switching losses, as shown in Table 2. The voltage-drop of SiC becomes higher as the temperature increases, while the Si counterpart reduces as the temperature rises. However, the voltage-drop of Si is almost 20 times the value of SiC at 25 °C, which demonstrates that the conduction loss of SiC is much smaller than that of Si. Therefore, the test results of both the dynamic and static characteristics of SiC show that the power losses of SiC are much smaller than the Si counterparts.

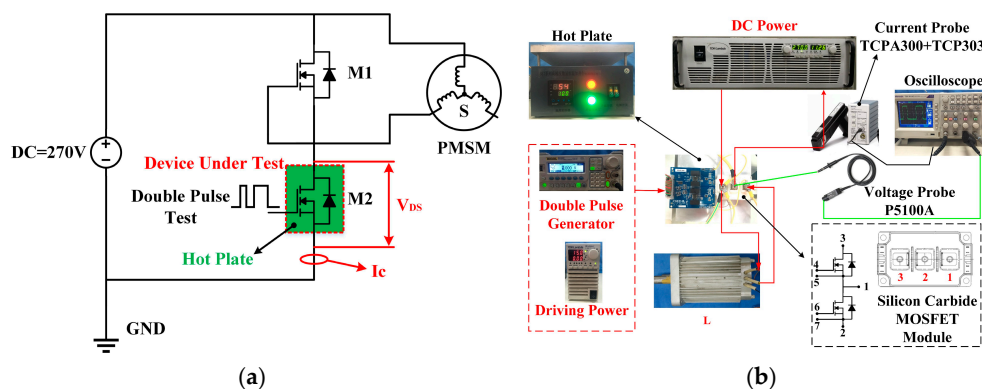


**Figure 3.** A double pulse test (DPT) bench. (a) Simplified DPT circuit; (b) Actual components in the test bench.

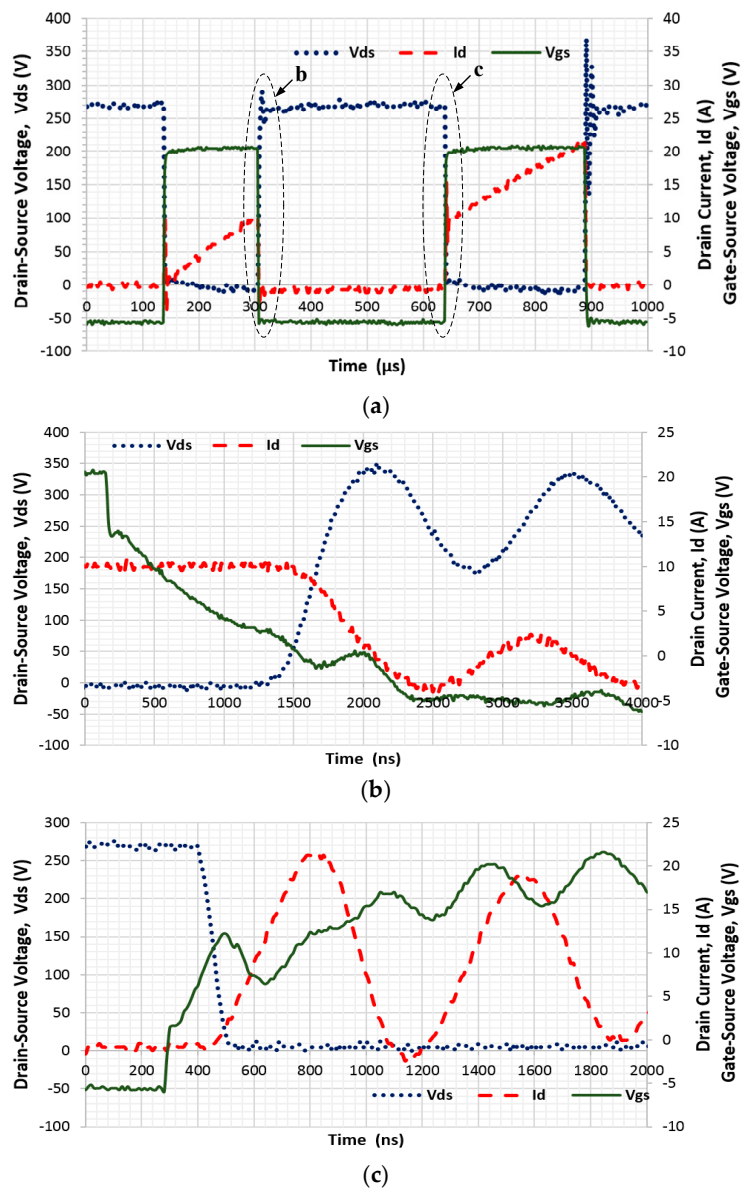


Figure 4. Switching transition waveform of SiC. (a) Total switching transition; (b) Turn-off transition; (c) Turn-on transition.

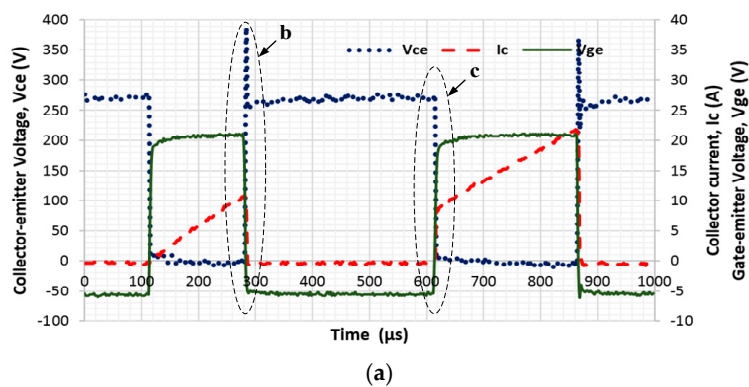
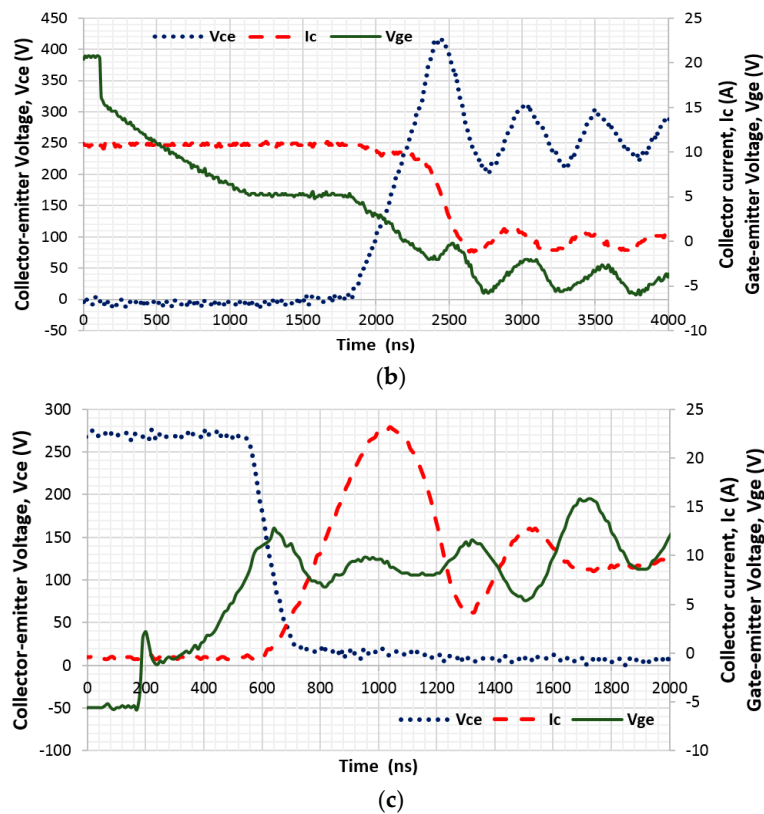


Figure 5. Cont.



**Figure 5.** Switching transition waveform of Si. (a) Total switching transition; (b) Turn-off transition; (c) Turn-on transition.

**Table 1.** Characteristic comparison between SiC and Si.

	SiC (Cree CAS300M12BM2)		Si Insulated-Gate Bipolar Transistor (IGBT) (Infineon FF400R12KE3)	
	25 °C	175 °C	25 °C	175 °C
DC voltage	270 V	270 V	270 V	270 V
Turn-on time	85 ns	79 ns	143 ns	145 ns
Turn-off time	153 ns	148 ns	328 ns	752 ns
On-state resistance	4.8 mΩ	7.84 mΩ	/	/
Collector-emitter saturation voltage	/	/	832.5 mV (9.5 A)	583.0 mV (9.4 A)
Output capacitance	12.7 nF	13.4 nF	32.7 nF	35.3 nF

**Table 2.** Voltage-drop comparison between SiC and Si under different temperatures.

Temperature	SiC (Cree CAS300M12BM2)		Si (Infineon FF400R12KE3)	
	$V_{ds}$	$I_d$	$V_{ce}$	$I_d$
25 °C	44.2 mV	9.2 A	832.5 mV	9.5 A
100 °C	60.1 mV	9.2 A	686.9 mV	9.3 A
175 °C	73.7 mV	9.4 A	583.0 mV	9.4 A

### 3. Efficiency of the Powertrain System

The efficiency of the powertrain system is investigated in this Section. An experimental setup for a powertrain system is shown in Figure 6. There are three main components in the powertrain, namely the DC/DC converter, inverter, and PMSM. The main losses are switching and conduction

losses of switching devices in both the DC/DC converter and the inverter, and iron loss and copper loss in the PMSM.

Both the voltages and currents of the DC/DC converter and DC/AC inverter are measured, respectively, by a Power Analyzer. Then, the efficiencies of both the converter and the inverter are obtained. Meanwhile, the output torque and speed of the motor are measured by a dynamometer, which are employed in the calculation of the efficiency of the PMSM.

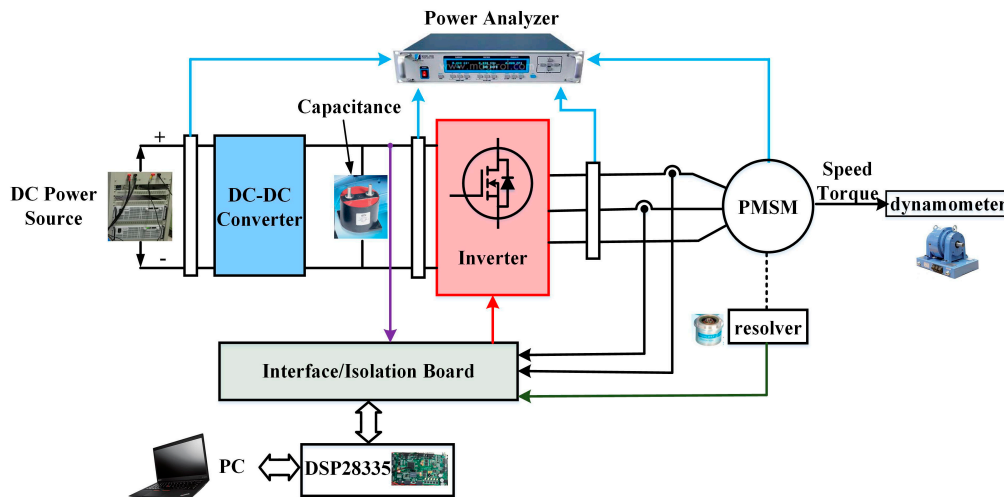


Figure 6. The structure of the experimental setup.

### 3.1. Efficiency of a Buck-Boost DC/DC Converter

The fundamental topology of a buck-boost DC/DC converter is shown in Figure 7. The buck-boost converter consists of two SiC MOSFETs (or Si IGBTs), two parallel diodes, an inductance, and two capacitors. The switching loss and conduction loss of SiC are the main contributions for the power losses of the DC/DC converter. The switching losses can be expressed as a function of the integration voltage and current during commuted intervals,

$$E_{\text{switching}} = E_{T_{\text{on}}} + E_{T_{\text{off}}} = \int_{t_1}^{t_2} V_{\text{ds}} \cdot I_{\text{d}} dt + \int_{t_3}^{t_4} V_{\text{ds}} \cdot I_{\text{d}} dt \quad (1)$$

where  $E_{T_{\text{on}}}$  and  $E_{T_{\text{off}}}$  are the turn-on and turn-off losses, respectively.  $t_1$ ,  $t_2$ ,  $t_3$ , and  $t_4$  represent the start and end of turn-on and turn-off, respectively. The switching losses of Si can be calculated the same as those of SiC.

The conduction loss of SiC can be calculated directly by the current and voltage,

$$P_{\text{conduction}} = I_{\text{d}}^2 \cdot R_{\text{ds(on)}} = V_{\text{ds}} \cdot I_{\text{d}} \quad (2)$$

Additionally, the power losses of the converter also contain the loss of inductance resistance and the capacitors' equivalent series resistances (ESR). Hence, the total losses, namely the efficiency of the converter, can be measured and calculated as follows,

$$\eta_{\text{converter}} = (U_2 \cdot i_2) / (U_1 \cdot i_1) \quad (3)$$

where  $U_1$  and  $U_2$  are the input and output voltages of the converter, respectively.  $i_1$  and  $i_2$  are the input and output currents of the converter, respectively.

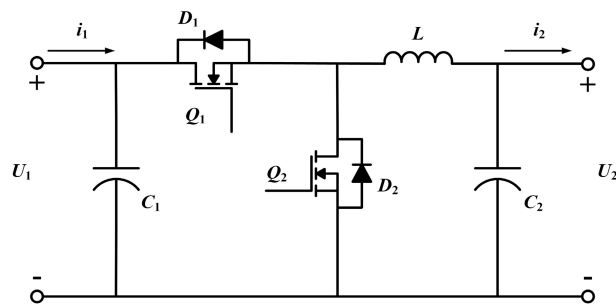


Figure 7. Topology of the DC/DC converter.

Figure 8 shows the efficiency comparison between the SiC- and Si-converters. The blue curve and black curve are measured by the experiments while the red curve and yellow curve are fitted based on the measured results. The peak efficiency of the SiC-inverter is nearly 93% at the output power of 30 kW, which is approximate 1% higher than that of the Si-converter.

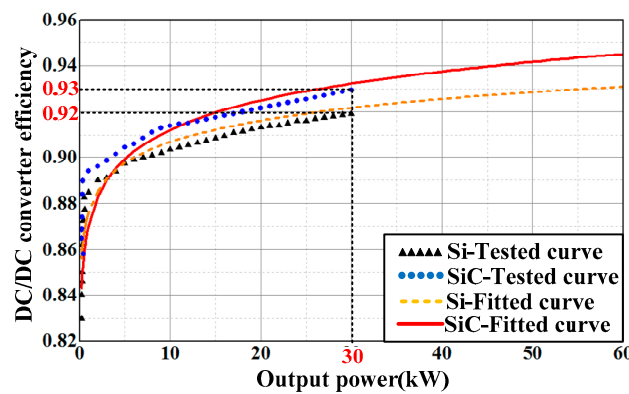


Figure 8. Efficiency comparison between the Si- and SiC-converters.

### 3.2. Efficiency of Inverter-PMSM

Figure 9 shows the fundamental topology of the DC/AC inverter and PMSM. The inverter contains six SiC MOSFETs (or Si IGBTs), six parallel diodes, one capacitor, etc. The switching loss and conduction loss of SiC are the main contributions for the power losses of the inverter, which is the same as that of the DC/DC converter. The loss model of the inverter can be found in Ref. [24–26]. This Section presents the measurement method and the test results.

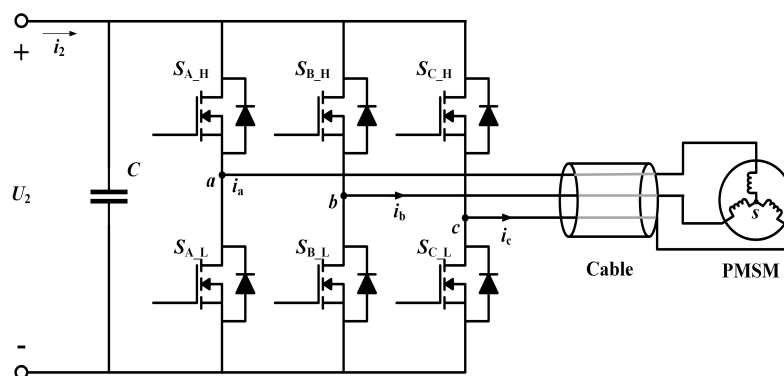


Figure 9. Topology of the DC/AC inverter-permanent magnet synchronous motor (PMSM).

The input power of the inverter is equal to the output power of the converter, as shown in Equation (4). The output power of the inverter is equal to the input power of the motor. The measurement method is shown in Figure 10.  $i_a$ ,  $i_b$ ,  $i_c$  represent the currents of Phase A, Phase B, and Phase C, respectively.  $U_{ab}$ ,  $U_{bc}$ ,  $U_{ac}$  are the three line-line voltages. Hence, the expression of the output power of the inverter is shown in Equation (5). The efficiency of the inverter can be calculated according to Equation (6).

$$P_{\text{input}} = U_2 \cdot i_2 \quad (4)$$

$$P_{\text{output}} = U_{ac} \cdot i_a + U_{bc} \cdot i_b \quad (5)$$

$$\eta_{\text{inverter}} = (U_{ac} \cdot i_a + U_{bc} \cdot i_b) / (U_2 \cdot i_2) \quad (6)$$

For the PMSM, the output power is mechanical energy, which is measured by a dynamometer. Hence, the efficiency of the motor is expressed as

$$\eta_{\text{motor}} = T \cdot n / [9.55(U_{ac} \cdot i_a + U_{bc} \cdot i_b)] \quad (7)$$

where  $T$  is the output mechanical torque of the motor and  $n$  is the mechanical speed of the motor.

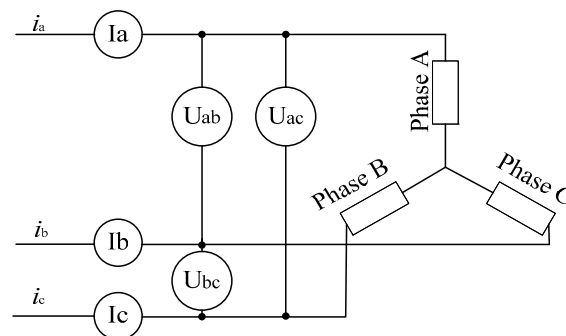


Figure 10. Measurement points of the DC/AC inverter.

The waveforms of Phase A and the  $\alpha\beta$  currents are shown in Figure 11. It is clearly seen that the currents of the Si-drive system include more harmonic components, which will induce more power losses in the motor. The phase current is dependent on the output phase voltage of the inverter. The distortions of the phase voltage are contributed by the voltage-drop, turn-on time and turn-off time of the switching devices, and the dead time of the phase leg [27–29]. The voltage-drop, turn-on time, and turn-off time of SiC MOSFETs are smaller than their Si IGBTs counterparts, which were measured and are shown in Tables 1 and 2 of Section 2 in this paper. Meanwhile, the shorter dead time could be set in the SiC-drive due to the faster turn-on and turn-off speed. Therefore, the distortions of the phase voltage of the Si-drive are more than the SiC-drive counterparts, resulting in more harmonic components in the current of the Si-drive system.

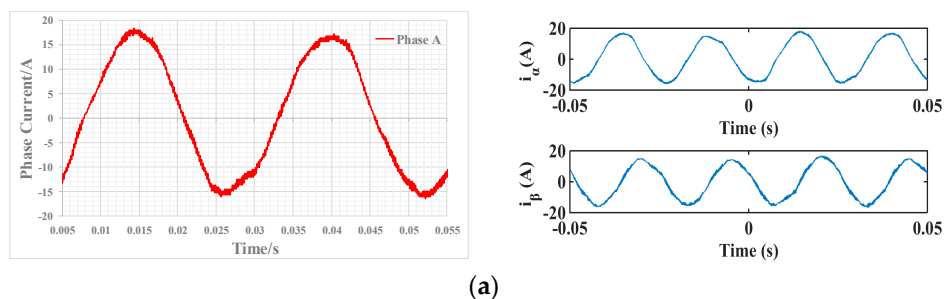
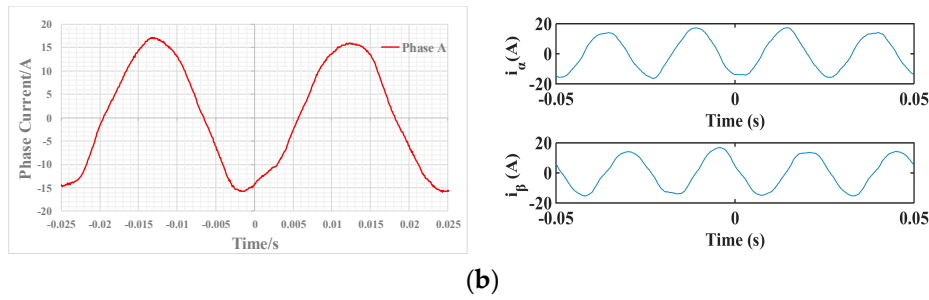


Figure 11. Cont.



**Figure 11.** Phase current and  $\alpha\beta$  current waveforms under 800 rpm and 8 N·m of the motor. (a) Current waveforms of the Si-drive system; (b) Current waveforms of the SiC-drive system.

There are two main losses in the motor, namely core losses in the iron core and copper losses in the winding. Both the core losses and copper losses include two parts; one part is induced by the fundamental current, and the other part is induced by the harmonic currents [24,30–32]. The core losses in the motor are composed of the eddy current loss  $P_e$  and hysteresis loss  $P_h$ . Both types of losses are caused by variation of the flux density in the core. Bertotti's model [30] is shown as,

$$P_c = P_e + P_h = k_e \sum_{n=1}^{\infty} (n\omega_1)^2 B_{p,n}^2 + k_h \sum_{n=1}^{\infty} (n\omega_1) B_{p,n}^x \quad (8)$$

where  $k_e$  and  $k_h$  are the eddy loss coefficient and the hysteresis loss coefficient, respectively,  $\omega_1$  is the fundamental angular frequency of the applied voltage, and  $n$  is the order of the harmonic. The peak flux density of the  $n$ th-order harmonic  $B_{p,current,n}$  due to the  $n$ th-order current is predicted by [31],

$$B_{p,current,n} = \mu_0 \frac{2W}{\pi\delta} \sum_{n=1}^{\infty} I_n \sum_v \frac{1}{v} K_{sov} K_{dpv} F_v(r) \quad (9)$$

The copper losses also include the fundamental component loss and the losses related with the harmonic currents [32]. The harmonics induce eddy currents in the conductors, which cause a non-uniform distribution of the current density within the cross-sectional area of each conductor. Such non-uniform distribution of the current density in a conductor according to its own current is called the skin effect, while that according to the currents in adjacent conductors is called the proximity effect. The expression of the copper losses can be written as follows [32],

$$P_{cu} = I_{rms}^2 R_{dc} + \sum_{h=3}^{\infty} I_n^2 R_{n,ac} \quad (10)$$

where  $I_{rms}$  is the rms current,  $R_{dc}$  is the dc resistance, and  $I_n$  is the rms current of the  $n$ th current.  $R_{n,ac}$  is the value of the  $n$ th harmonic resistance, which is determined by its dc value  $R_{dc}$  multiplying the ac skin and proximity gain,

$$R_{n,ac} = R_{dc} (K_{n,se} + K_{n,pe}) \quad (11)$$

where  $K_{n,se}$  is the  $n$ th resistance gain caused by the skin effect, and  $K_{n,pe}$  is the  $n$ th resistance gain caused by the proximity effect. Therefore, the phase current of the Si-drive system includes more harmonic components, resulting in more power losses in the motor.

Meanwhile, the amplitude of the phase current in the Si-drive system is higher than the SiC-system counterpart when the output powers of the two systems are the same. Hence, the efficiencies of both the inverter and the motor in the SiC-drive system are higher than the Si-system counterpart as shown in Figure 12. As a result, the efficiency of the overall inverter-motor system based on SiC is higher than that of the Si-system, especially with light loads.

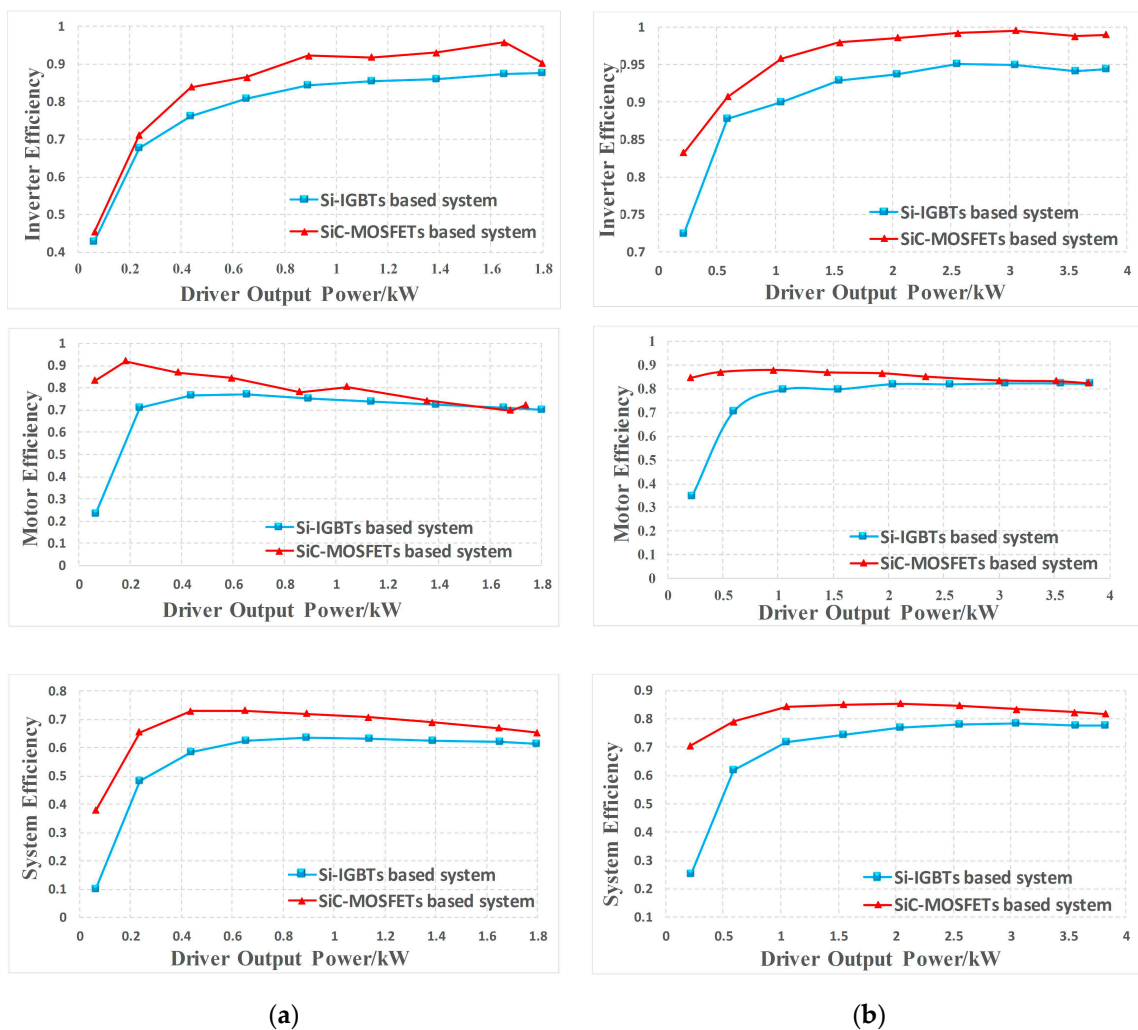


**Figure 12.** Efficiency comparison of Si and SiC based inverter-motor systems under different output powers. (a) 400 rpm; (b) 1000 rpm.

Due to the limited power rating of the dynamometer in our lab, the efficiency of the overall inverter-motor system during the full power range is expanded from the limited tested results shown in Figure 13, which will be adopted in the next Section. When the speed was smaller than 800 rpm and the torque was below 350 N·m, the efficiency of the overall inverter-motor system was measured by experiments. Then the range of the efficiency was expanded when the speed was higher than 800 rpm and the torque was bigger than 350 N·m through fitting formulas. There are several fitting algorithms to fit formulas based on MATLAB, such as Gaussian, Interpolant, Polynomial, Wei bull, etc. Among these fitting methods, the formulas fitted by the Polynomial had the best fitting degree, and the optimal fitting degree was 0.9682. Hence, the polynomial was adopted and the corresponding fitting formulas are shown as Equations (12) and (13), respectively.

$$\eta = 0.01941n^3 - 0.01153n^2T - 0.001971nT^2 + 0.0205T^3 - 0.0405n^2 + 0.02037nT - 0.02738T^2 + 0.006666n - 0.0154T + 0.9134 \quad (12)$$

$$\eta = 0.02362n^3 - 0.01249n^2T - 0.0010351nT^2 + 0.02103T^3 - 0.05183n^2 + 0.02005nT - 0.02814T^2 - 0.007325n - 0.0152T + 0.953 \quad (13)$$

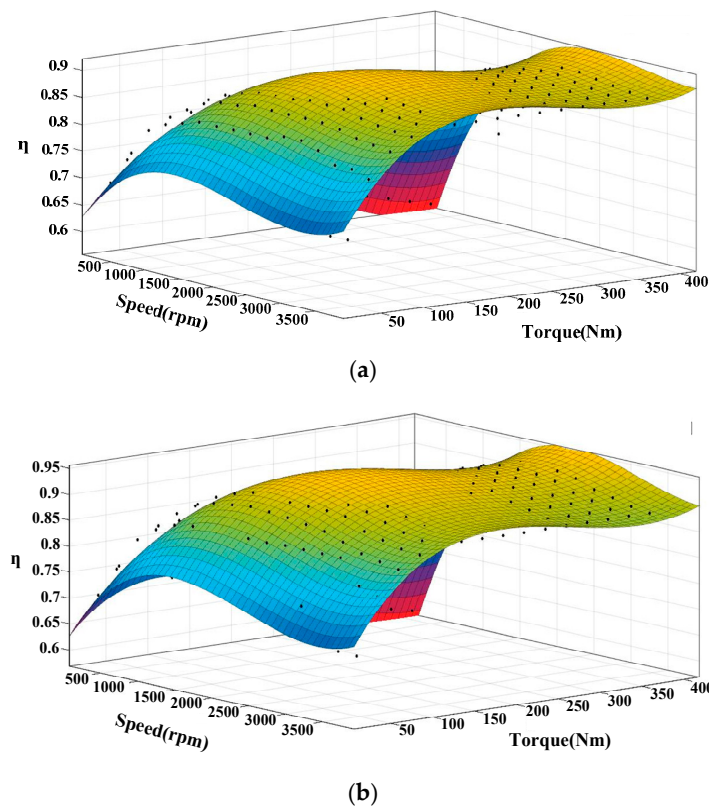


**Figure 13.** Efficiency comparison of Si and SiC based inverter-motor systems under full power range. (a) Si-system; (b) SiC-system.

#### 4. Simulations in ADVISOR

The ADVISOR software provides a simulation environment based on MATLAB for EVs. The powertrain architecture of an EV in ADVISOR is shown in Figure 14. The efficiencies of the motor, inverter, and converter could be assigned to the motor and control module, respectively. Then, the comprehensive comparison between the SiC based powertrain and the Si based powertrain is implemented through the simulations. The U.S. Environmental Protection Agency Urban Dynamometer Driving Schedule (UDDS) cycle was adopted in these simulations. UDDS represents city driving conditions for a light duty vehicle as shown in Figure 15. Two typical topologies are investigated, namely Topology A: battery-inverter-motor, and Topology B: battery-converter-inverter-motor.

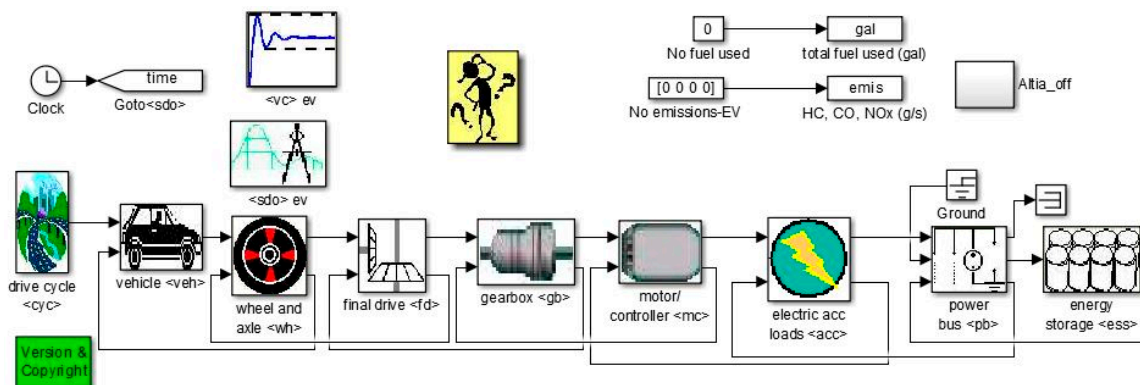


**Figure 14.** Powertrain architecture of the Electric Vehicle in ADVISOR.

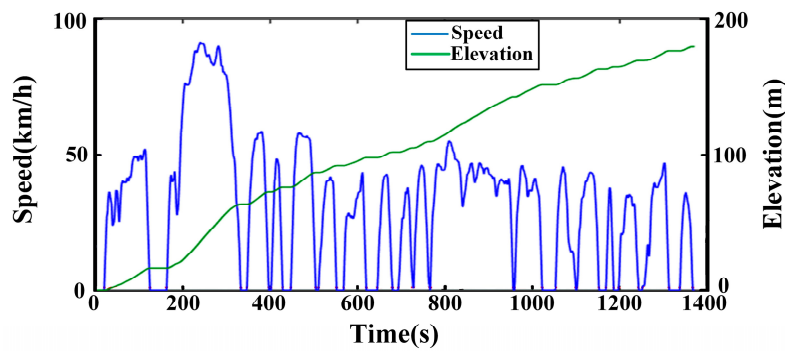


Figure 15. Urban Dynamometer Driving Schedule (UDDS) cycle.

4.1. Topology A: Battery-Inverter-Motor

The topology A is shown in Figure 16, which consists of battery, DC/AC inverter and PMSM. The efficiency contours and actual operating points for the Si- and SiC-inverter-motor systems in ADVISOR are shown in Figure 17, which are drawn based on the experimental results. The efficiency of the SiC-inverter-motor system is higher than the Si-system counterpart during the full power range. Hence, the power loss of the SiC-inverter-motor system is much smaller than that of the Si-system during the total UDDS cycle as shown in Figure 18. Meanwhile, the SOC of the battery in the SiC-system is also higher than that in the Si-system due to the higher efficiency of the SiC-inverter-motor system shown in Figure 19. The quantified results are given in Tables 3 and 4.



Figure 16. Topology A: Battery-inverter-PMSM.

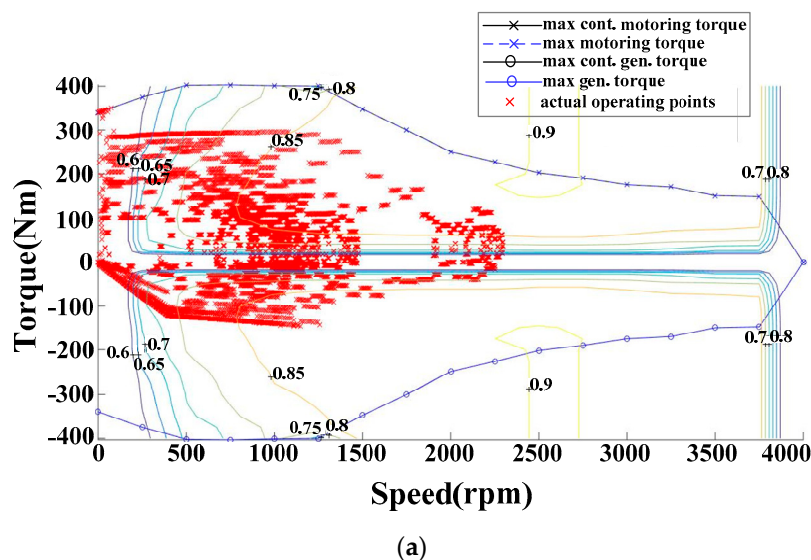
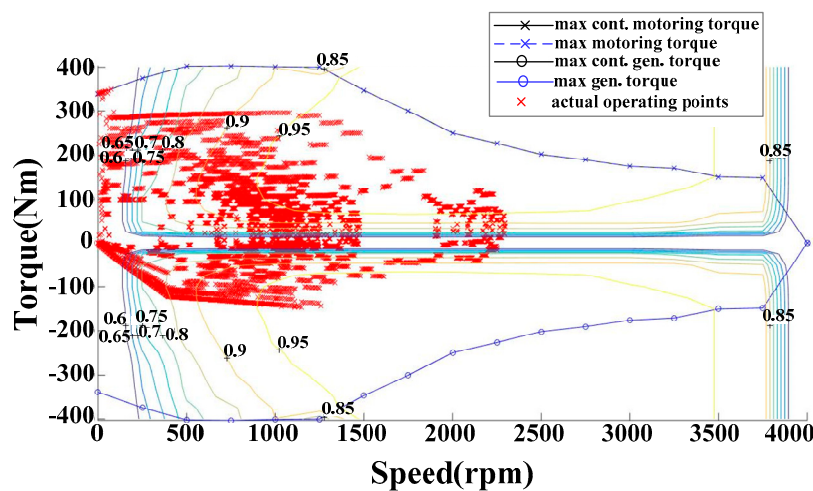


Figure 17. Cont.



(b)

Figure 17. The efficiency contours and actual operating points of the Si- and SiC-inverter-motor system at different speeds and different torques. (a) Si-inverter-motor system; (b) SiC-inverter-motor system.

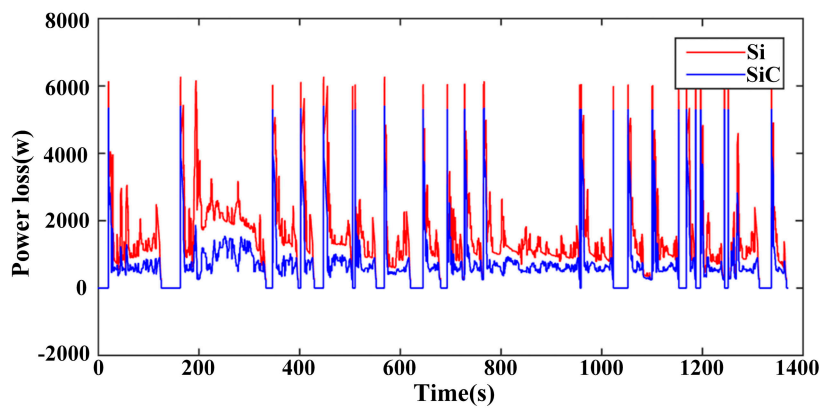


Figure 18. Power loss comparison of the SiC- and Si-inverter-motor systems.

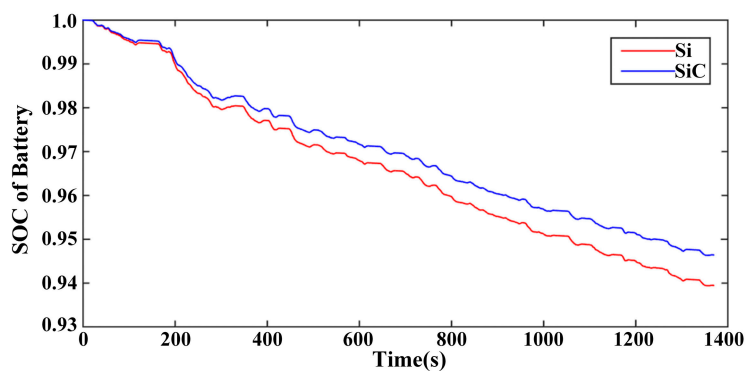


Figure 19. Battery SOC comparison of the SiC- and Si-inverter-motor systems.

Different elevations are considered, namely 0, 1.5%, 3.0%, and 4.5%. All the power consumptions in the SiC-system are smaller than those in the Si-system, as shown in Tables 3 and 4. When the elevation is 0, the improvements of equivalent fuel, output energy of the battery, braking energy recuperated, and efficiency of the overall system are 12.50%, 8.85%, 14.98%, and 13.00%, respectively.

Such incredible enhancements are due to the higher efficiency and more sinusoidal waveform phase current of the SiC-inverter-motor system.

Additionally, the higher elevation increases the power consumption due to more output torque required. For example, the output energy of the battery in the SiC system is 15,307 KJ when the elevation is 4.5%, while the output energy of the battery is 9783 KJ when the elevation is 1.5%.

**Table 3.** Comparison of SiC- and Si-systems at zero elevation for Topology A.

Description	SiC (Cree CAS300M12BM2)	Si Insulated-Gate Bipolar Transistor (IGBT) (Infineon FF400R12KE3)	Improve (%)
Elevation	0	0	-
Equivalent fuel (L/100 km)	2.1	2.4	12.50
Drive distance (km)	12	12	-
Output energy of battery (kJ)	7285	7992	8.85
Efficiency of inverter-motor system (%)	87.5	79	10.76
Braking energy recuperated (kJ)	990	861	14.98
Efficiency of overall system (%)	36.5	32.3	13.00

**Table 4.** Comparison of SiC- and Si-systems at 1.5%, 3.0%, and 4.5% elevations for Topology A.

Description	SiC (Cree CAS300M12BM2)			Si IGBT (Infineon FF400R12KE3)		
	1.5	3	4.5	1.5	3	4.5
Elevation	1.5	3	4.5	1.5	3	4.5
Equivalent fuel (L/100 km)	2.9	3.7	4.5	3.2	4.1	5
Drive distance (km)	12	12	12	12	12	12
Output energy of battery (kJ)	9783	12,480	15,307	10,736	13,719	16,847
Efficiency of inverter-motor system (%)	88.4	89.9	91.06	81.37	82.75	83.56
Braking energy recuperated (kJ)	742	559	442	631	484	365
Efficiency of overall system (%)	25.6	19.4	15.5	22.9	17.7	14

#### 4.2. Topology B: Battery-Converter-Inverter-Motor

In this section, the DC/DC converter is taken into account. The topology is shown in Figure 20. There are the battery, DC/DC converter, DC/AC inverter, and PMSM in the powertrain system. Actually, many EV powertrain systems adopt this topology, which can easily adjust the DC voltage in the system. The efficiency of the SiC-converter-inverter-motor system is higher than the Si-system counterpart during the full power range, which is the same as topology-B. Hence, the power loss of the SiC-converter-inverter-motor system is much smaller than that of the Si-system during the total UDDS cycle, as shown in Figure 21. Additionally, the battery SOC for the SiC-system is higher than that of the Si-system, as shown in Figure 22. The quantified results are summarized in Tables 5 and 6.

For topology B, four scenarios are also considered, namely 0, 1.5%, 3.0%, and 4.5% elevations. The output energy of the battery in the SiC-system is smaller than those of the Si-system for every case shown in Tables 5 and 6. Its improvement is 14.31%, which is more than the improvement of 8.85% for topology A. The improvements of the other parameters of topology B, such as equivalent fuel, efficiency of the converter-inverter-motor, braking energy recuperated, and efficiency of the overall system, are all higher than their counterparts of topology A, which is due to taking the SiC DC/DC converter into account in the powertrain system. Its efficiency is higher than that of the Si DC/DC converter. Table 6 also shows that the higher the elevation, the more power consumption is needed.

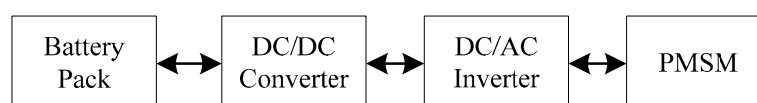


**Figure 20.** Topology B: Battery-converter-inverter-PMSM.

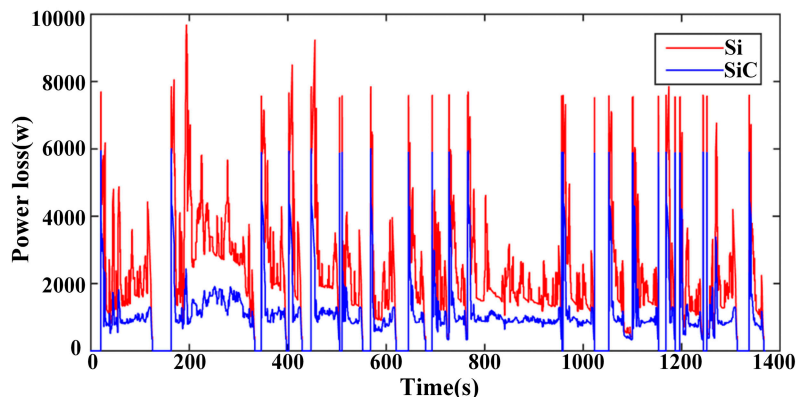


Figure 21. Power loss comparison of the SiC- and Si-converter-inverter-motor systems.

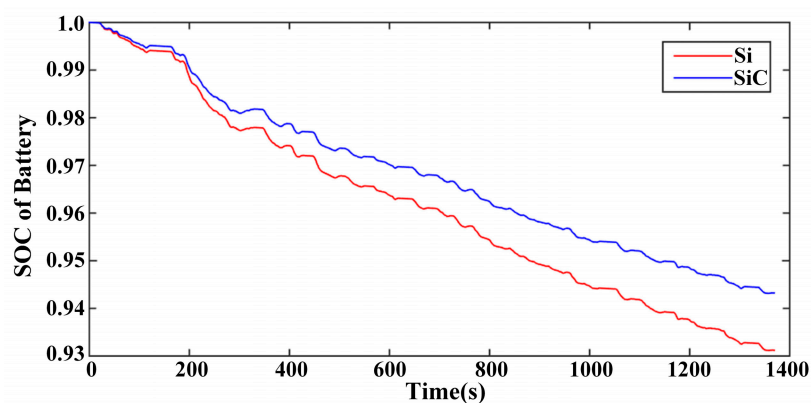


Figure 22. Battery SOC comparison of the SiC- and Si-converter-inverter-motor systems.

Table 5. Comparison of the SiC- and Si-systems at zero elevation for Topology B.

Description	SiC (Cree CAS300M12BM2)	Si IGBT (Infineon FF400R12KE3)	Improve (%)
Elevation	0	0	-
Equivalent fuel (L/100 km)	2.2	2.6	15.38
Drive distance (km)	12	12	-
Output energy of battery (kJ)	7599	8821	14.31
Efficiency of converter-inverter-motor system (%)	83.59	70.94	17.83
Braking energy recuperated (kJ)	915	696	31.47
Efficiency of overall system (%)	34.4	28.4	21.14

Table 6. Comparison of the SiC- and Si-systems at 1.5%, 3.0%, and 4.5% elevations for Topology B.

Description	SiC (Cree CAS300M12BM2)			Si IGBT (Infineon FF400R12KE3)		
	1.5	3	4.5	1.5	3	4.5
Elevation	1.5	3	4.5	1.5	3	4.5
Equivalent fuel (L/100 km)	3	3.8	4.7	3.5	4.5	5.5
Drive distance (km)	12	12	12	12	12	12
Output energy of battery (kJ)	10,148	12,897	15,765	11,778	15,009	18,382
Efficiency of converter-inverter-motor system (%)	86.51	88.41	89.62	73.7	75.25	76.26
Braking energy recuperated (kJ)	681	511	383	514	386	287
Efficiency of overall system (%)	24.4	18.7	15	20.5	15.8	12.7

## 5. Conclusions

This paper comprehensively investigated the impact of SiC power devices on the powertrain of EVs. The characteristics of SiC were measured and demonstrated outstanding advantages, such

as faster switching speed, lower voltage drop, and more stability than the Si counterparts. Hence, both the DC/DC converter and DC/AC inverter based on SiC exhibited higher efficiency than that of the Si systems. Furthermore, there are low harmonic components in the phase currents of the SiC-system. Therefore, the high efficiency of the motor benefits from the more sinusoidal waveform of the phase current.

Two typical topologies of drive systems were analyzed by ADVISOR. Both topologies A and B based on SiC represented remarkable enhancements of the performances, such as smaller equivalent fuel consumption, smaller output energy of the battery, more efficiency and braking energy recuperated, etc. The smaller output energy of the battery, higher efficiency, and more braking energy recuperated means that EVs could adopt a smaller battery pack, reduce their weight, increase cruise distance, etc. Therefore, this work is meaningful for improving the performances of EVs.

**Acknowledgments:** This work was supported in part by the National Natural Science Foundation of China under Project 51407004 and in part by the Aeronautical Science Foundation of China 20162851016.

**Author Contributions:** Xiaofeng Ding proposed the main idea for this paper and wrote this paper. Jiawei Cheng did the simulation and drew the related figures. Feida Chen evaluated the characteristics of the devices by the experiments. All authors carried out the theoretical analysis and contributed to writing the paper.

**Conflicts of Interest:** The authors declare no conflict of interest.

## References

1. Shamsi, P.; McDonough, M.; Fahimi, B. Wide-Bandgap Semiconductor Technology: Its impact on the electrification of the transportation industry. *IEEE Electr. Mag.* **2013**, *1*, 59–63. [[CrossRef](#)]
2. Hamada, K.; Nagao, M.; Ajioka, M.; Kawai, F. SiC—Emerging Power Device Technology for Next-Generation Electrically Powered Environmentally Friendly Vehicles. *IEEE Trans. Electr. Devices* **2015**, *62*, 278–285. [[CrossRef](#)]
3. Xiong, R.; Sun, F.; Chen, Z. A data-driven multi-scale extended Kalman filtering based parameter and state estimation approach of lithium-ion polymer battery in electric vehicles. *Appl. Energy* **2014**, *113*, 463–476. [[CrossRef](#)]
4. Ruan, J.; Walker, P.; Zhang, N. A comparative study energy consumption and costs of battery electric vehicle transmissions. *Appl. Energy* **2016**, *165*, 119–134. [[CrossRef](#)]
5. Zhang, Y.; Xiong, R.; He, H.; Shen, W. A lithium-ion battery pack state of charge and state of energy estimation algorithms using a hardware-in-the-loop validation. *IEEE Trans. Power Electr.* **2017**, *32*, 4421–4431. [[CrossRef](#)]
6. Jagemont, J.; Boulon, L.; Dubé, Y. A comprehensive review of lithium-ion batteries used in hybrid and electric vehicles at cold temperatures. *Appl. Energy* **2016**, *164*, 99–114. [[CrossRef](#)]
7. Sun, F.; Xiong, R.; He, H. A systematic state-of-charge estimation framework for multi-cell battery pack in electric vehicles using bias correction technique. *Appl. Energy* **2016**, *162*, 1399–1409. [[CrossRef](#)]
8. Pohlenz, D.; Böcker, J. Efficiency improvement of an IPMSM using Maximum Efficiency operating strategy. In Proceedings of the 2010 14th International Power Electronics and Motion Control Conference (EPE/PEMC), Ohrid, Macedonia, 6–8 September 2010; pp. 15–19.
9. Shang, F.; Arribas, A.P.; Krishnamurthy, M. A comprehensive evaluation of SiC devices in traction applications. In Proceedings of the 2014 IEEE Transportation Electrification Conference and Expo (ITEC), Dearborn, MI, USA, 15–18 June 2014; pp. 1–5.
10. Zhang, H.; Tolbert, L.M.; Ozpineci, B. Impact of SiC Devices on Hybrid Electric and Plug-In Hybrid Electric Vehicles. *IEEE Trans. Ind. Appl.* **2011**, *47*, 912–921. [[CrossRef](#)]
11. Jahdi, S.; Alatise, O.; Fisher, C.; Ran, L.; Mawby, P. An Evaluation of Silicon Carbide Unipolar Technologies for Electric Vehicle Drive-Trains. *IEEE J. Emerg. Sel. Top. Power Electr.* **2014**, *2*, 517–528. [[CrossRef](#)]
12. Kassakian, J.G.; Jahns, T.M. Evolving and Emerging Applications of Power Electronics in Systems. *IEEE J. Emerg. Sel. Top. Power Electr.* **2013**, *1*, 47–58. [[CrossRef](#)]
13. Wang, F.; Zhang, Z.; Ericson, T.; Raju, R.; Burgos, R.; Boroyevich, D. Advances in Power Conversion and Drives for Shipboard Systems. *Proc. IEEE* **2015**, *103*, 2285–2311. [[CrossRef](#)]
14. Tanimoto, S.; Matsui, K. High Junction Temperature and Low Parasitic Inductance Power Module Technology for Compact Power Conversion Systems. *IEEE Trans. Electr. Devices* **2015**, *62*, 258–269. [[CrossRef](#)]

15. Xu, F.; Guo, B.; Xu, Z.; Tolbert, L.M.; Wang, F.; Blalock, B.J. Paralleled Three-Phase Current-Source Rectifiers for High-Efficiency Power Supply Applications. *IEEE Trans. Ind. Appl.* **2015**, *51*, 2388–2397. [[CrossRef](#)]
16. Josifović, I.; Popović-Gerber, J.; Ferreira, J.A. Improving SiC JFET Switching Behavior under Influence of Circuit Parasitics. *IEEE Trans. Power Electr.* **2012**, *27*, 3843–3854. [[CrossRef](#)]
17. Sun, K.; Wu, H.; Lu, J.; Xing, Y.; Huang, L. Improved Modeling of Medium Voltage SiC MOSFET within Wide Temperature Range. *IEEE Trans. Power Electr.* **2014**, *29*, 2229–2237. [[CrossRef](#)]
18. Brown, C.D.; Sarlioglu, B. Reducing Switching Losses in BLDC Motor Drives by Reducing Body Diode Conduction of MOSFETs. *IEEE Trans. Ind. Appl.* **2015**, *51*, 1864–1871. [[CrossRef](#)]
19. Swamy, M.M.; Kang, J.; Shirabe, K. Power Loss, System Efficiency, and Leakage Current Comparison between Si IGBT VFD and SiC FET VFD with Various Filtering Options. *IEEE Trans. Ind. Appl.* **2015**, *51*, 3858–3866. [[CrossRef](#)]
20. Shirabe, K.; Swamy, M.; Kang, J.K.; Hisatsune, M.; Das, M.; Callanan, R.; Lin, H. Design of 400 V class inverter drive using SiC 6-in-1 power module. In Proceedings of the 2013 IEEE Energy Conversion Congress and Exposition (ECCE), Denver, CO, USA, 15–19 September 2013; pp. 2363–2370.
21. Merkert, A.; Krone, T.; Mertens, A. Characterization and Scalable Modeling of Power Semiconductors for Optimized Design of Traction Inverters with Si- and SiC-Devices. *IEEE Trans. Power Electr.* **2014**, *29*, 2238–2245. [[CrossRef](#)]
22. Zhao, T.; Wang, J.; Huang, A.Q.; Agarwal, A. Comparisons of SiC MOSFET and Si IGBT Based Motor Drive Systems. In Proceedings of the Conference Record of the 2007 IEEE Industry Applications Conference, 42nd IAS Annual Meeting, New Orleans, LA, USA, 23–27 September 2007; pp. 331–335.
23. Reed, J.K.; McFarland, J.; Tangudu, J.; Vinot, E.; Trigui, R.; Venkataramanan, G.; Gupta, S.; Jahns, T. Modeling power semiconductor losses in HEV powertrains using Si and SiC devices. In Proceedings of the 2010 IEEE Vehicle Power and Propulsion Conference (VPPC), Lille, France, 1–3 September 2010; pp. 1–6.
24. Ding, X.F.; Liu, G.L.; Du, M.; Guo, H.; Duan, C.W.; Qian, H. Efficiency Improvement of Overall PMSM-Inverter System Based on Artificial Bee Colony Algorithm Under Full Power Range. *IEEE Trans. Mag.* **2016**, *52*, 1–4. [[CrossRef](#)]
25. Hassan, W.; Wang, B. Efficiency optimization of PMSM based drive system. In Proceedings of the 2012 7th International Power Electronics and Motion Control Conference (IPEMC), Harbin, China, 2–5 June 2012; Volume 2.
26. Mestha, L.K.; Evans, P.D. Analysis of on-state losses in PWM inverters. *Electr. Power Appl. IEE Proc. B* **1989**, *136*, 189–195. [[CrossRef](#)]
27. Choi, J.W.; Sul, S.K. Inverter output voltage synthesis using novel dead time compensation. *IEEE Trans. Power Electr.* **1996**, *11*, 221–227. [[CrossRef](#)]
28. Zhang, Z.; Xu, L. Dead-Time Compensation of Inverters Considering Snubber and Parasitic Capacitance. *IEEE Trans. Power Electr.* **2014**, *29*, 3179–3187. [[CrossRef](#)]
29. Bedetti, N.; Calligaro, S.; Petrella, R. Self-Commissioning of Inverter Dead-Time Compensation by Multiple Linear Regression Based on a Physical Model. *IEEE Trans. Ind. Appl.* **2015**, *51*, 3954–3964. [[CrossRef](#)]
30. Boglietti, A.; Cavagnino, A.; Lazzari, M.; Pastorelli, M. Predicting iron losses in soft magnetic materials with arbitrary voltage supply: An engineering approach. *IEEE Trans. Magn.* **2003**, *39*, 981–989. [[CrossRef](#)]
31. Zhu, Z.Q.; Howe, D. Instantaneous magnetic field distribution in permanent magnet brushless DC motors. IV. Magnetic field on load. *IEEE Trans. Magn.* **1993**, *29*, 152–158. [[CrossRef](#)]
32. Key, T.S.; Lai, J.S. Costs and benefits of harmonic current reduction for switch-mode power supplies in a commercial office building. *IEEE Trans. Ind. Appl.* **1996**, *32*, 1017–1025. [[CrossRef](#)]

